Nanoscale

Accepted Manuscript

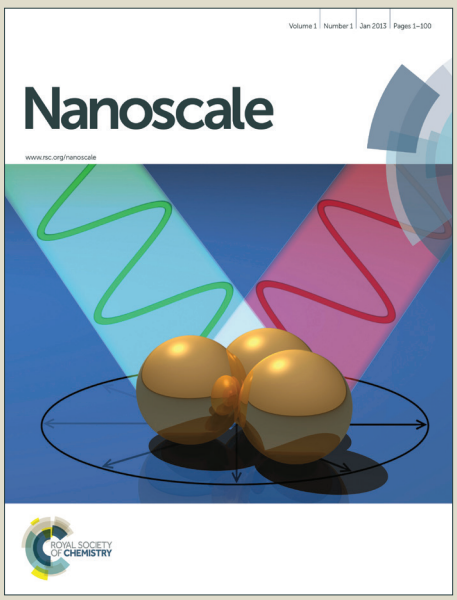

ROYAL SOCIETY OF CHEMISTRY

www.rsc.org/nanoscale

Nanoscale

RSCPublishing

ARTICLE

Size-Controlled Silver Nanoparticles Stabilized on Thiol-Functionalized MIL-53(Al) Frameworks

Cite this: DOI: 10.1039/x0xx00000x

Xinquan Cheng,[a] Min Liu,*[a] Anfeng Zhang,[a] Shen Hu,[a] Chunshan Song,[a,b] Guoliang Zhang,[c] Xinwen Guo*[a]

Received 00th January 2015,
Accepted 00th January 2015

DOI: 10.1039/x0xx00000x

www.rsc.org/

A postsynthetic modification method was used to prepare thiol-functionalized metal organic framework (MOF) by the amidation of mercaptoacetic acid with the amine group, which contains in the frameworks of NH_2-MIL-53(Al). By doing this, thiol group has been successfully grafted on the framework of MOF, which perfectly combined the highly developed pore structures of MOF with the strong coordination ability of thiol group. The resulting thiol-functionalized MIL-53(Al) showed a significantly high adsorption capacity to heavy metal ions like Ag^+ (182.8 mg/g). Even more important, these grafted thiol groups can be used as anchoring groups for stabilizing metal nanoparticles (NPs) with controllable sizes. Take silver as an example, monodispersed Ag NPs encapsulated in the cages of MIL-53(Al) have been prepared by using a two-step procedure. In addition, the particle size of the Ag NPs was adjustable to some extent by controlling the initial loading amount. The average size of the smallest Ag NPs is 3.9 ± 0.9 nm, which is hard to obtain for Ag NPs because of their strong tendency to aggregate.

Introduction

Metal organic frameworks (MOFs) are compounds built from the coordination of metal ions or clusters with organic ligands to form one-, two-, or three-dimensional pore structures.[1-3] MOFs have received much of the initial interest and enthusiasm from researchers mainly contributed from their high surface areas and hence extremely high capacity to capture various kinds of gases, such as carbon dioxide,[4, 5] hydrogen,[6] and methane[7] etc. Indeed, through the past few decades, MOFs have done an excellent job in these related areas. However, MOFs also have various structures and properties that came from almost infinite combinations of metals and ligands. As a result, along with this prominent interest in gas absorption, other potential applications of MOFs have begun to flourish in diverse areas, including catalysis,[8-10] biotechnology,[11-14] sensing,[15, 16] and nonlinear optics.[17] In order to develop the applications of MOFs in these fields, the development of MOFs that possess complex chemical and physical properties is becoming the core work. Since MOFs have highly developed pore structures and easily tunable physicochemical properties, postsynthetic modification (PSM) became one of the most efficient methods to achieve chemical modification of MOFs. By targeting the organic ligand or the metal ion that is composed of the MOF, one can exploit various chemical reactions available to transform the current MOF into a new MOF with other functional groups, and thus changing its physical and chemical properties.

According to the definition of Cohen,[18] postsynthetic modification of MOFs can be mainly divided into three approaches: (a) covalent PSM, (b) dative PSM, (c) postsynthetic deprotection (PSD). This definition is based on which type of chemical bond is formed or broken during the postsynthetic process. For covalent PSM, a new covalent bond is formed between a reaction reagent and a component of the MOF that is generally the organic linker of the MOF. However, dative PSM occurs through the formation of a new dative bond with a component of the MOF. Finally, in PSD a reaction is performed on MOF to cleave a chemical bond within an intact framework of the MOF. This method has been less widely explored as a postsynthetic approach.

To date, there are many successful examples of covalent and dative PSM of MOFs. Qiu and co-workers[19] demonstrated a dative PSM way to cooperate thiol group into the frameworks of MOF by using dithioglycol to coordinate with the coordinatively unsaturated copper centers of HKUST-1. The resulting thiol-functionalized MOF has very strong ability to remove heavy metal ion of Hg^{2+} from water. In covalent PSM, usually a functional group within MOFs is picked as the target to form covalent bond with the reaction reagent. Amine group have been used more extensively as the target of modification than any other functional groups.[18] For instance, Nguyen and Cohen[20] described that hydrophobic properties could easily be incorporated into MOFs by grafting the long alkyl groups within amine containing frameworks. In this approach, a series of

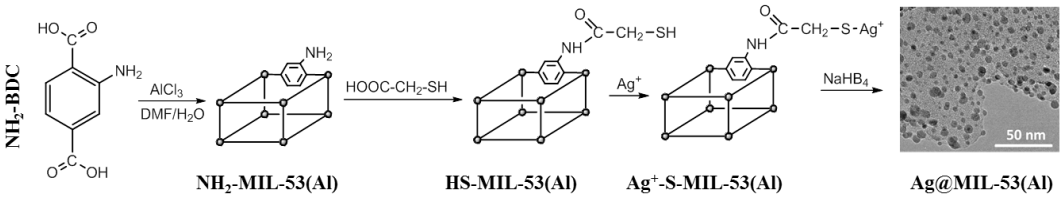

Scheme 1. Scheme for the fabrication of HS-MIL-53(Al) and Ag@MIL-53(Al) by postsynthetic modification of NH_2-MIL-53(Al)

unstable hydrophilic IRMOFs became hydrophobic materials, which could stable exist in ambient air and even in water. In addition, the robust NH_2-MIL-53(Al) was transformed into a superhydrophobic material by them in the same way. Caro and co-workers[21] showed a covalent PSM method to prepare ZIF-90 molecular sieve membranes, by using 3-aminopropyltriethoxysilane as a covalent linker to combine the ZIF-90 layer with Al_2O_3 support via imines condensation, which greatly increased the thermal and hydrothermal stabilities of ZIF-90 membranes. Rosseinsky *et al*.[22] reported the condensation of salicylaldehyde with IRMOF-3, which is a porous MOF decorated with pendant amine groups. By doing this, a good metal chelator salicylidene group was attached to the framework and it was available for subsequent coordinate with other metal ions. This important finding proved that installation of strong metal chelators onto the frameworks of MOFs by covalent PSM did not impact its structural integrity. Moreover, this finding also showed us an indirect way to prepare MOFs containing certain kinds of metal ions, which is hard to form MOFs by directly coordinate them with organic ligands.

Inspired by these inventions, we proposed a PSM approach to synthesize thiol-functionalized MOF (HS-MOF) by the amidation of mercaptoacetic acid with the amine groups that contain in the frameworks of NH_2-MIL-53(Al). Consequently, thiol group has been successfully grafted on the frameworks of MIL-53(Al). Considering the way to obtain HS-MOF, our approach is a covalent PSM and it is different from the method used by Qiu and co-workers[19] which is a dative PSM. In addition, the application of HS-MOF is different. Qiu and co-workers mainly used their HS-MOF to remove heavy metal ions, but our HS-MOF can not only do so. More important, it can be used as host matrix to fabricate metal nanoparticles (NPs) with adjustable size, by using the stabilized ability of thiol group to prevent further aggregation.[23, 24]

In order to fabricate metal NPs with controllable size, by taking silver as an example, a two-step procedure was introduced (Scheme 1). Firstly, thiol-functionalized MIL-53(Al) (HS-MIL-53(Al)) was used to adsorb certain amounts of silver ions in water solution. Then, a weaker reducing agent like $NaBH_4$ was used to reduce these captured silver ions, which resulted in the formation of Ag NPs encapsulated in the frameworks of MIL-53(Al). By controlling the whole process carefully, monodispersed Ag NPs were obtained, and the particle size could be reduced from average 5.3 ± 1.2 nm to 3.9 ± 0.9 nm by limiting the initial amounts of Ag^+ being adsorbed. The resulting Ag NPs were encapsulated in the frameworks of MIL-53(Al), but were still accessible for other reagents due to the high porosity of the matrix. Many literatures showed that metal NPs encapsulated in MOFs were useful in various areas, such as heterogeneous catalysis,[25-30] gas adsorption[32-33] and chemical sensing.[34-36] Therefore, this type of monodispersed and size-controlled Ag NPs may be applied in catalysis and gas adsorption with high performance. Furthermore, we believe that monodispersed Pt NPs and Pd NPs could be prepared by the same method.

Experimental

Materials and chemicals

2-Amino-1, 4-Benzenedicarboxylic acid (NH_2-BDC) and mercaptoacetic acid were purchased from Aldrich. Aluminium(Ⅲ) chloride hexahydrate ($AlCl_3 \cdot 6H_2O$), silver nitrate, toluene, sodium borohydride, anhydrous ethanol, N,N-dimethylformamide (DMF), and dimethyl ketone were obtained from Shanghai Chemical Reagent Inc. of the Chinese Medicine Group. Deionized water was purchased from Dalian University of Technology. All chemicals were used as received without further purification.

Synthesis of NH_2-MIL-53(Al)

Based on our previous works,[37] NH_2-MIL-53(Al) crystals with different sizes, morphologies and properties were obtained just by altering the ratio of water in the DMF-water mixed solvent system. In this article, two types of NH_2-MIL-53(Al) crystals were chosen as matrices to do PSM. They are named matrix 1 (**M1**) and matrix 2 (**M2**), which were synthesized from pure deionized water and DMF-water mixed solvents containing 6.7 vol% of deionized water, respectively. In a typical synthesis, 0.56 g (3.1 mmol) of NH_2-BDC and 0.76 g (3.1 mmol) of $AlCl_3 \cdot 6H_2O$ were dissolved in DMF or deionized water separately. The ratio of the mixed solvents might change, while the total volume of solvents was kept constant at 30 mL. Then, the two separate solutions were mixed together. After that, the mixture was placed in a 100 mL Teflon-lined steel autoclave and heated for 24 hours in an oven at 150 ℃ under static conditions. The resulting solid products were activated in boiling DMF for 5 hours to remove the remaining water molecules or unreacted organic linkers trapped in the pores.[38] After filtering and washing with dimethyl ketone, the resulting white powders were dried overnight in a vacuum oven at 30 ℃.

HS-PSM of NH_2-MIL-53(Al)

M1 and **M2** were used as matrices for PSM of thiol group (HS-PSM). In a common procedure, 0.3 g (1.0 mmol) of NH_2-MIL-53(Al) crystals, 15 mL of mercaptoacetic acid (216.6 mmol) and 15 mL of toluene were added in a glass flask. The mixture was stirred under reflux for 6 hours at 120 ℃. The product was recovered by repeated centrifugation and washed with dimethyl ketone in order to remove those unreacted mercaptoacetic acid molecules trapped in the frameworks, and then dried overnight in a vacuum oven at 30 ℃. The resulting product was named as HS-MIL-53(Al), and it was abbreviated as HS-X. HS- denotes the MIL-53(Al) frameworks were grafted with thiol group, and X represents different kinds of matrices. For example, when using **M1** as the matrix for HS-PSM, the resulting product should be named as HS-M1.

Fabrication of Ag NPs

Several kinds of Ag NPs were prepared according to the following two-step procedure. First, 0.1 g (~0.27 mmol) of HS-MIL-53(Al) and 60 mL aqueous solution containing certain amounts of silver ions were placed in a 100 mL flask and stirred at room temperature for 3 hours. Because of the strong coordination ability of thiol group with silver ions, Ag^+-S-MIL-53(Al) was formed within the mixture. The resulting solid was washed six times with water in order to removing the physisorption of silver ions on the surface, and then washed with a great amount of ethanol to remove water molecules. Second, the solid was dispersed in 100 mL of ethanol at 0 ℃, and then 100 mL of ethanol solution of sodium borohydride (30 mg, 0.79 mmol) was added to reduce these captured silver ions to metallic silvers under 0 ℃ for 3 hours. The resulting products were washed by ethanol for six times and dried overnight in a vacuum oven at 30 ℃ before further analysis. The final product was named as Ag@X, which X represents the initial kinds of matrices, and Ag@ means these Ag NPs were encapsulated in the cages of the matrix. For instance, when **M2** was used as the initial matrix to support Ag NPs, the resulting product should be named as Ag@M2.

Characterization methods

Transmission electron microscopy (TEM) images were taken by a FEI Technai 30F electron microscopy operated at 200 kV. The samples were prepared by placing a drop of the dimethyl ketone solution of Ag@X onto a continuous carbon-coated copper grid, followed by removal of excess solution with absorbent paper and dried at ambient condition. Powder X-ray diffraction (XRD) patterns were recorded on a Rigaku SmartLab(9) diffractometer with a scanning rate of 6 °/min between 5 ° and 50 °. Cu Ka obtained at 40 kV of tube voltage and 100 mA of current was used as the X-ray source. Temperature dependent XRD (TDXRD) measurements were also carried out on this same equipment using an in-situ reactor named XRK-900. The temperature of the reactor was raised from 50 ℃ to 500 ℃ with an interval of 50 ℃. During this process, the TDXRD patterns were collected at each specific temperature. N_2 adsorption/desorption isotherms were recorded at −196 °C on a Quantachrom Autosorb-iQ instrument. Before measurement, samples were degassed at 130 ℃ overnight. Thermogravimetric and differential thermal analysis (TG-DTA) was obtained from a Rigaku TG-8120 instrument in the temperature range of 25−900 °C under nitrogen atmosphere, at a heating rate of 4 ℃/min. The UV-vis diffuse reflection spectroscopy (UV-vis DRS) was recorded on a JASCO V-550 spectrophotometer. X-ray photoelectron spectroscopy (XPS) measurements were performed on a Kratos AXIS Ultra DLD spectrometer using a monochromatic Al K_α (1486.6 eV) irradiation source operated at 150 W. Spectrometer pass energies of 160 eV for the survey spectra and 20 eV for high resolution spectra of all elemental spectral regions. The density of thiol group was estimated from the sulfur content determined by elemental analysis on varioEL Ⅲ (elementar company). The mass loading ratio of silver and the concentration of silver solution were measured by inductively coupled plasma atomic emission spectroscopy (ICP-AES) on an Optima 2000DV analyzer.

Results and Discussion

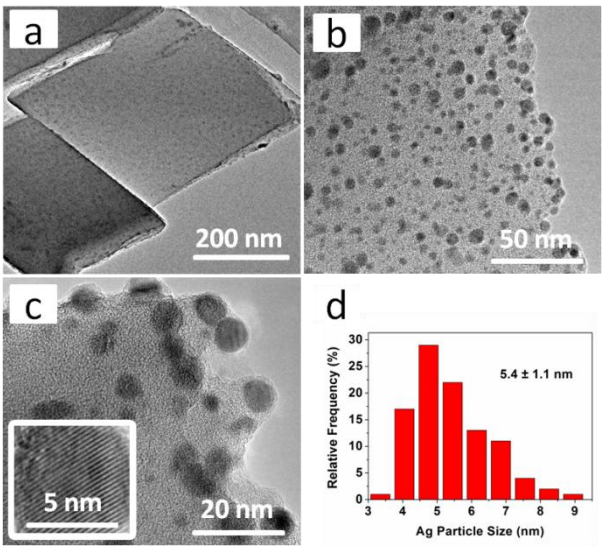

Fig. 1 TEM images of Ag@M1 at different magnifications and its corresponding particle size distribution pattern.

The TEM images (Fig. 1a, b) revealed formation of homogeneous dispersed Ag NPs throughout the bulk of the MOF matrix, and the lattice fringe of the Ag NPs could be seen clearly (Fig. 1c). The average particle size is 5.4 ± 1.1 nm, and exhibiting a relative narrow size distribution (Fig. 1d). Apparently, this particle size is much larger than the narrow pore apertures of **M1** (0.8 nm).[39] However, there are several reasons to prove that these Ag NPs were embedded into the matrix instead of on the surface. First of all, the initial amine groups were pending in the frameworks of NH_2-MIL-53(Al), and then thiol groups were grafted on these sites, so the thiol groups were pending in the frameworks. After that, these thiol groups were used as anchoring groups to capture Ag^+. Then, the captured Ag^+ were reduced to metallic silvers. Meanwhile, the Ag NPs were formed through the agglomeration of the nearby small silver particles. Therefore, the Ag NPs should end up within the

frameworks.[40] Secondly, the saturation adsorption capacity of HS-M1 to Ag^+ is 89.2 mg/g, which is much higher than the adsorption capacity of the matrix **M1** (2.1 mg/g), so the majority amount of Ag^+ being adsorbed were contributed to the thiol groups. In addition, we implement strict processes to remove those Ag^+ that were physically adsorbed on the surface before reduction. Hence, the vast majority amounts of the resulting Ag NPs were incorporated in the frameworks of the matrix. According to the classification method of Fischer et al.,[41, 42] this kind of metal particles supported on MOFs belongs to the class B, which means metal particles were distributed throughout the volume of the MOF matrices, but were exhibiting a particle size characteristically larger than the dimensions of the pores of the matrices. The important thing is, although the Ag NPs were encapsulated in the matrix with a particle size larger than the matrix's pore, they were still accessible for other reagents due to the highly developed pore structures of the matrix.

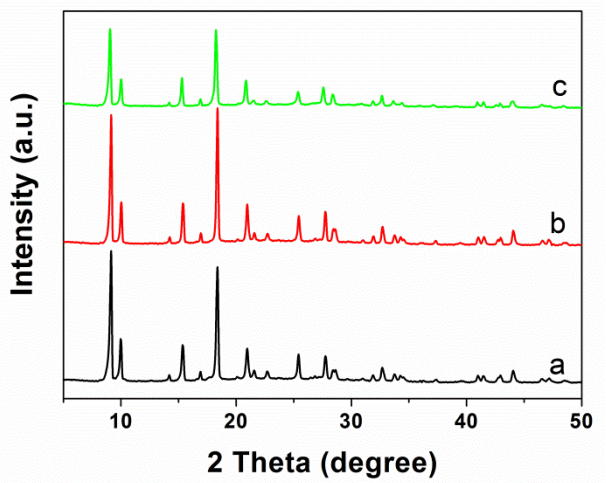

Fig. 2 XRD patterns of (a) **M1**; (b) HS-M1; and (C) Ag@M1.

The framework structure of all products was identified by XRD (Fig. 2), it turned out that they have a very similar pattern that corresponds to the MIL-53(Al) structure. This structure contains chains of μ-OH corner-sharing AlO_6-octahedra, which are interconnected by NH_2-BDC molecules to form its pore structure.[38] The almost unchanged X-ray diffraction patterns between **M1** and thiol-functionalized **M1** showed that the thiol group grafting occurs with no apparent loss of crystallinity, which indicates that the integrity of the matrix's frameworks was well-retained (Fig. 2b). Even after a large amount of silver loaded, the crystalline structure was still maintained, but the intensities of the diffraction peaks were greatly reduced (Fig. 2c). This could correspond to the adsorption effects of the Ag NPs to X-ray, which is a common phenomenon in metal NPs incorporated in the frameworks of MOFs.[43] Interestingly, no supplementary Bragg peaks appeared belong to the Ag NPs (Fig. 2c), which is another common phenomenon in metal NPs supported on MOFs.[43] The main reason was due to the monodispersed Ag NPs were too small to be detected by the X-ray diffraction.

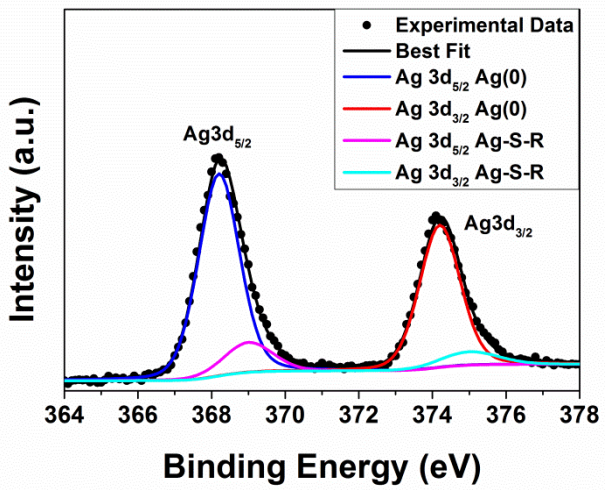

Fig. 3 XPS spectrum of Ag@M1.

However, the X-ray photoelectron spectroscopy (XPS) could determine the oxidation state of the Ag NPs. Fig. 3 shows two spin-orbit pairs of components, by following a rigorous curve-fitting procedure. The main signal of $Ag3d_{5/2}$ is centered at 368.2 eV, as expected for metallic silver atoms in the bulk phase of Ag NPs.[44-46] Another spin-orbit pair with a binding energy around 369 eV, which is attributed to the silver atoms bonding with thiol groups through the S-bridge (Ag-S-R), as reported in the literatures.[47, 48] The splitting of the Ag3d doublet is 6 eV, which means the $Ag3d_{3/2}$ peaks appeared at 374.2 eV and 375 eV, respectively for metallic silver atoms and silver atoms bonding with thiol groups. The branching ratio of $Ag3d_{5/2}$ to $Ag3d_{3/2}$ is about 1.5, which is calculated by the integration of the peak areas. All these data matched very well with the literatures,[44-48] indicating the metallic nature of this kind of Ag NPs. Therefore, the XPS analysis confirmed our expectation that this kind of silver supported on the matrix **M1** is mainly metallic silver and stabilized by the thiol groups.

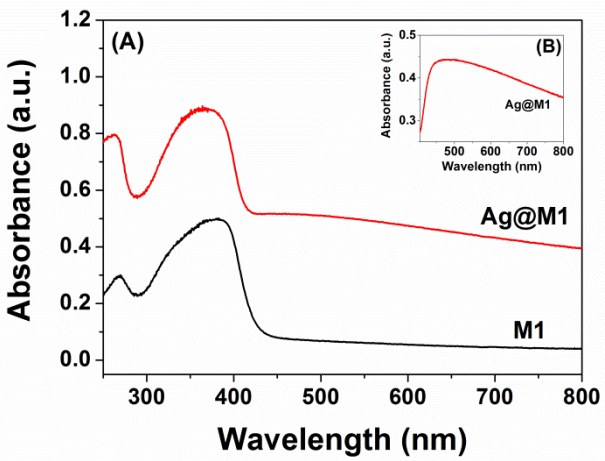

Fig. 4 UV-vis diffuse reflectance spectra of (A) **M1** and Ag@M1; (B) Ag@M1 in the visible light region by subtraction of the spectrum of **M1**.

Table 1 Capacity to Ag^+, content of thiol group, the resulting particle size of Ag NPs with a different loading amount, and nitrogen sorption data

Sample	Capacity to Ag^+ before HS-PSM (mg/g)[a]	Content of –SH after HS-PSM (%)[b]	Capacity to Ag^+ after HS-PSM (mg/g)[a]	S_{BET} (m^2/g)[d]	S_{micro} (m^2/g)[d]	S_{ex} (m^2/g)[d]	V_{micro} (cm^3/g)[d]	V_{total} (cm^3/g)[d]
M1	2.1	14.7	89.2	994	567	427	0.39	0.87
M2	3.6	26.4	182.8	2610	2209	401	1.03	1.83
	Ag loading amount (wt%)[a]		Ag particle size (nm)[c]					
Ag@M2	7.4		3.9 ±0.9	1304	952	352	0.42	1.18
	15.4		5.3 ±1.2	496	154	342	0.08	0.71

[a] Measured by ICP-AES, and the initial concentration of Ag^+ solution is 423.3 mg/L. [b] Determined by elemental analyser. [c] Obtained from TEM by counting one hundred particles. [d] Measured by N_2 adsorption at −196 °C, and the total pore volumes have been calculated at a p/p_0 value of 0.995.

The UV-vis DRS spectra of matrix **M1** and Ag@M1 are shown in Fig. 4. As observed in Fig. 4A, the matrix **M1** only exhibited obvious absorption in the UV region with an absorption edge around 450 nm, but there was no more absorption in visible wavelengths. Notably, the Ag@M1 showed significant enhancement of light absorption than the matrix **M1** both in the UV and visible light regions. By subtraction of the matrix spectrum from the spectrum of Ag@M1, we can clearly see a broad absorption in the visible light region (Fig. 4B). This strong and broad absorption centered at around 470 nm could be attributed to the surface plasmon band of Ag NPs, as suggested in the literatures.[45, 49] The above UV-vis DRS results are in agreement with the TEM and XPS analysis, and further proved that the silver species encapsulated in the MOF matrix is metallic silver.

Since the Ag NPs were formed by aggregation of small particles from the nearby sites, the resulting particle sizes should be adjustable by controlling the loading extent. In order to prove that in a more efficient way, a sample with higher adsorption capacity to Ag^+ would be better. According to our previous works,[37] the size and morphology of the matrix could be controlled just by altering the ratio of water in the DMF-water mixed solvent system. Meanwhile, the resulting crystals' BET surface areas were quite different. Moreover, the experiment showed that the matrix with a higher BET surface areas resulting in a higher density of thiol group after HS-PSM, which led to a higher adsorption capacity to Ag^+. Through multiple experiments, a perfect ratio of water (6.7 vol%) in the mixed solvent was determined, which would lead to a type of NH_2-MIL-53(Al) crystals with a total BET surface areas of 2610 m^2/g (Table 1). This value is higher than our previous reported 1882 m^2/g under the water ratio of 3.3 vol%, and so far it is the highest BET value being reported for NH_2-MIL-53(Al) when compared with the normal value around 1000 m^2/g. Considering 2610 m^2/g surface area is an extremely high number and nitrogen physisorption is not satisfactory with regard to a quantitative assessment of the microporosity. Argon has been used as an alternative probe molecule to remeasure this sample since argon molecule is monatomic and less reactive than the diatomic nitrogen molecule.[50] The result exhibited a similar total BET surface area of 2817 m^2/g (Fig. S1†). Therefore this type of NH_2-MIL-53(Al) crystals has highly developed pore structure, and it has been chosen as the matrix 2 (**M2**) to do HS-PSM and to fabricate Ag NPs with controllable size. As a result, **M2** had a much higher density of thiol group than **M1** after grafting with thiol group by amidation reaction (Table 1). The resulting saturation adsorption capacity of HS-M2 to Ag^+ is 182.8 mg/g, which is more than twice as high as the adsorption quantity of HS-M1 (89.2 mg/g). This significantly higher adsorption capacity to Ag^+ is mainly contributed from the large amounts of thiol groups containing in its frameworks, and its highly developed pore structures were still available for other agents. Hence, HS-M2 should be high performance adsorbent for heavy metal ions since thiol group has strong coordination ability with plenty of heavy metal ions, such as Hg^{2+}, Cd^{2+}, Pd^{2+}, and Pt^{2+} *etc*. In addition, both matrix **M1** and **M2** are highly thermal stable. For the solvent-free structures of them, they can stable up to at least 320 ℃ (Fig. S2†), which would greatly extend the application of the Ag NPs supported on these matrices.

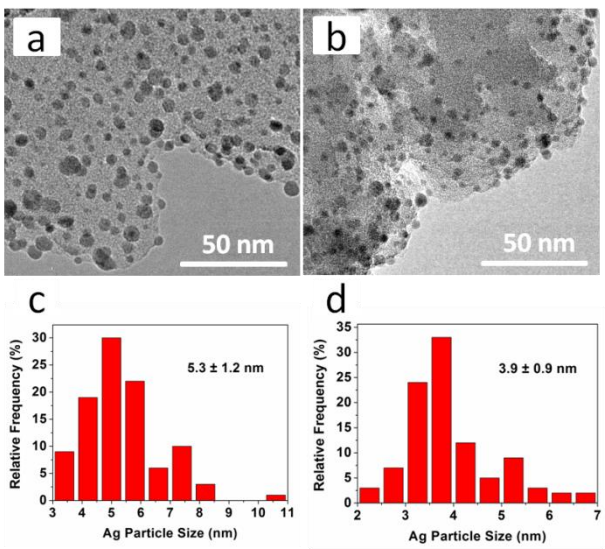

Fig. 5 TEM images of Ag@M2 and its corresponding particle size distribution patterns under different loading amount of silver: (a) and (c) 15.4 wt%; (b) and (d) 7.4 wt%.

Based on matrix **M2**, after the reduction of silver ions to metallic silvers, monodispersed Ag NPs encapsulated in the matrix (Ag@M2) were obtained (Fig. 5). Moreover, the resulting particle size of Ag NPs could be controlled to some extent by regulating the initial amounts of silver ions being adsorbed. The results showed that, by reducing the silver loading amount from 15.4 wt% to 7.4 wt%, the average diameter of the Ag NPs decreased from 5.3 ± 1.2 nm to 3.9 ± 0.9 nm (Table 1). Meanwhile, the Ag NPs became much sparse through the whole volume of the matrix. However, further lowering the loading amount would not reduce the particle size. The particles just became more scattered. The main reason is that small Ag NPs have strong tendency to aggregate with the nearby particles and form larger silver particles. Actually, the tendency to aggregate for Ag NPs is stronger than other kinds of metal NPs, and it is hard to fabricate Ag NPs smaller than 5 nm, according to literatures.[43, 51] Hence, Ag NPs incorporated in **M2** with an average size of 3.9 ± 0.9 nm may have great potentials for further applications in metal catalysis and hydrogen storage.

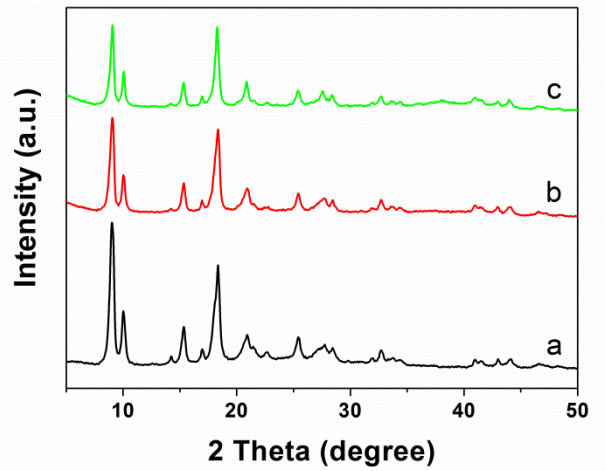

Fig. 6 XRD patterns of (a) **M2**; (b) 7.4 wt%-Ag@M2; and (c) 15.4 wt%-Ag@M2.

Nitrogen sorption measurements revealed that all the samples had a similar micropore adsorption/desorption isotherms (Fig. S1†), but their sorption data were quite different (Table 1). In the first place, by comparing **M2** to **M1**, we could see that **M2** has highly developed pore structure, and that is why **M2** has been chosen as the matrix to change the loading extent of silver in order to control the resulting particle sizes of Ag NPs. Secondly, when we compared **M2** to Ag@M2, it clearly showed that the total BET surface areas of **M2** had been greatly reduced from 2610 m^2/g to 1304 m^2/g after loading with 7.4 wt% of silver, and further decreased to 496 m^2/g by increasing the loading amount to 15.4 wt%. However, the external surface areas exhibited a slight change. Apparently, this kind of change is mainly contributed from the decreasing micropore surface areas. In addition, the micropore volumes also sharply decreased as the silver loading extent increased. These phenomena further proved that the Ag NPs were encapsulated in the cages of the matrix, not on the external surface. It is noteworthy that the matrix's micropore surface areas were greatly reduced after loading with silver, but it still cannot be ignored and the framework structure of the matrix was well preserved. Therefore, these Ag NPs can be accessible to other reagents. This important fact ensures the further applications of these Ag NPs.

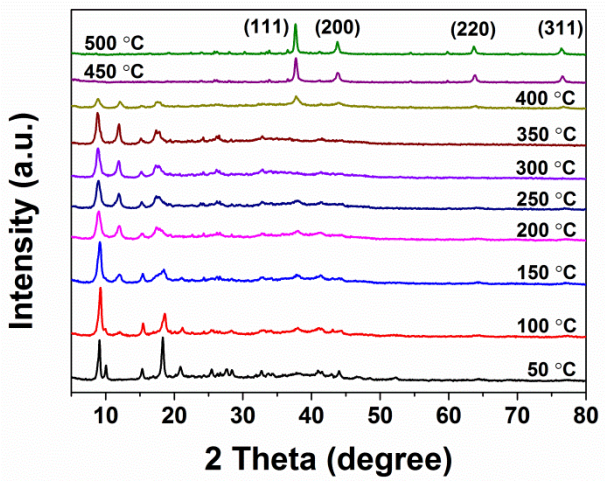

Fig. 7 TDXRD patterns of 15.4 wt%-Ag@M2.

The corresponding XRD patterns (Fig. 6) showed that the intensity of the reflection peaks falls gradually with the increasing loading amounts of silver. This is mainly contributed from the adsorption effects of Ag NPs to X-ray, but no obvious diffraction peaks of Ag NPs appeared, primarily because of the small particle size which has been proved by the TEM (Fig. 5). Also, the UV-vis DRS spectra can prove the existing of metallic silver nanoparticles (Fig. S3†). In addition, the framework structures were still well-remained even with a 15.4 wt% of silver loaded (Fig. 6c). The thermal stabilities of Ag@M2 and **M2** have been determined by the temperature dependent XRD measurements (Fig. 7, Fig. S4† and S5†). Fig. 7 is clearly shown that the framework structure of **M2** is stable up to 350 ℃. However, when raising the temperature to 400 ℃, the matrix's structure started to collapse, and the diffraction peaks belong to the Ag NPs begun to appear. After the temperature was increased to 450 ℃, the framework structure was completely collapsed and the diffraction peaks of Ag NPs became more obvious. These peaks were assigned to diffraction from the (111), (200), (220), and (311) planes of face-centered cubic silver, respectively.[52] Keep increasing the temperature to 500 ℃, the intensities of these diffraction peaks were increased. All these phenomena directly proved the previous inference that the Ag NPs were formed by aggregation of small particles. As raising the temperature, the particle size of the Ag NPs gradually increased. When the Ag NPs became large enough, they could show up on the XRD pattern with specific diffraction peaks. It is worth noting that there are minor changes in the XRD patterns with increasing the temperature, such as the peak at 2θ=10.0 ° disappeared gradually and the peak at 2θ=12.3 ° appeared. This is because MIL-53(Al) has breathing effect, and its structural flexibility is depending on the nature of guest molecules and temperature.[53, 54] Hence, its cell parameters will

change as the temperature varies, and it will reflect on the XRD pattern (Fig. S6†).

Conclusions

We have successfully demonstrated a postsynthetic method to prepare thiol-functionalized MIL-53(Al) by the amidation of mercaptoacetic acid with the amine group, which is contained in the frameworks of NH_2-MIL-53(Al). The resulting HS-MIL-53(Al) perfectly combined the highly developed pore structure of MIL-53(Al) with the strong coordination ability of thiol group, and showed a significantly high adsorption capacity to Ag^+ (182.8 mg/g). In addition, HS-MIL-53(Al) can be used as matrix to support Ag NPs, in which the thiol group acting as anchoring group to stabilize Ag NPs. By doing this, monodispersed Ag NPs encapsulated in the cages of the matrices have been prepared by using a solution impregnation method and subsequent reduction with $NaBH_4$. Although the Ag NPs were trapped in the frameworks of the matrices, they are still accessible for other reagents. Furthermore, the particle sizes of the Ag NPs are controllable to some extent by limiting the loading extent of silver. The average sizes of the Ag NPs can be reduced to 3.9 ± 0.9 nm. Since Ag NPs have strong tendencies to aggregate, the preparation of Ag NPs smaller than 5 nm is very difficultly. Therefore, these small Ag NPs are promising materials for heterogenous metal catalysis and gas adsorption.

Acknowledgements

This work was supported by the State Key Program of National Natural Science Foundation of China (Grant No. 21236008).

Notes and references

[a] *State Key Laboratory of Fine Chemicals, PSU-DUT Joint Center for Energy Research, School of Chemical Engineering, Dalian University of Technology, Dalian 116024, P. R. China. Fax: +86-0411-84986134; Tel: +86-0411-84986133, +86-0411-84986134; E-mail: guoxw@dlut.edu.cn, lium@dlut.edu.cn*
[b] *EMS Energy Institute, PSU-DUT Joint Center for Energy Research and Department of Energy & Mineral Engineering, Pennsylvania State University, University Park, Pennsylvania 16802, United States. Fax: 814-865-3573; Tel: 814-863-4466; E-mail:csong@psu.edu*
[c] *College of Biological and Environmental Engineering, Zhejiang University of Technology, Hangzhou 310014, P. R. China. Fax: +86-0571-88320863; Tel: +86-0571-88320863; E-mail: guoliangz@zjut.edu.cn*

† Electronic Supplementary Information (ESI) available: Consists of Nitrogen and Argon adsorption/desorption isotherms, TG and DTG curves, UV-vis diffuse reflectance spectra, temperature dependent XRD patterns, and XRD patterns. See DOI: 10.1039/b000000x/

1 O. M. Yaghi, M. O'Keeffe, N. W. Ockwig, H. K. Chae, M. Eddaoud and J. Kim, *Nature*, 2003, **423**, 705-714.
2 S. M. Cohen, *Chem. Rev.*, 2012, **112**, 970-1000.
3 N. Stock and S. Biswas, *Chem. Rev.*, 2012, **112**, 933-969.
4 K. Sumida, D. L. Rogow, J. A. Mason, T. M. McDonald, E. D. Bloch, Z. R. Herm, T. H. Bae and J. R. Long, *Chem. Rev.*, 2012, **112**, 724-781.
5 J. Liu, P. K. Thallapally, B. P. McGrail, D. R. Brown and J. Liu, *Chem. Soc. Rev.*, 2012, **41**, 2308-2322.
6 N. L. Rosi, J. Eckert, M. Eddaoudi, D. T. Vodak, J. Kim, M. O'Keeffe and O. M. Yaghi, *Science*, 2003, **300**, 1127-1129.
7 H. Wu, W. Zhou and T. Yildirim, *J. Am. Chem. Soc.*, 2009, **131**, 4995-5000.
8 M. Yoon, R. Srirambalaji and K. Kim, *Chem. Rev.*, 2012, **112**, 1196-1231.
9 M. Gustafsson, A. Bartoszewicz, B. n. Martín-Matute, J. Sun, J. Grins, T. Zhao, Z. Li, G. Zhu and X. Zou, *Chem. Mater.*, 2010, **22**, 3316-3322.
10 Y. Fu, D. Sun, Y. Chen, R. Huang, Z. Ding, X. Fu and Z. Li, *Angew. Chem., Int. Ed.*, 2012, **51**, 3364-3367.
11 J. Della Rocca, D. Liu and W. Lin, *Accounts Chem. Res.*, 2011, **44**, 957-968.
12 S. Keskin and S. Kızılel, *Ind. Eng. Chem. Res.*, 2011, **50**, 1799-1812.
13 A. C. McKinlay, R. E. Morris, P. Horcajada, G. Ferey, R. Gref, P. Couvreur and C. Serre, *Angew. Chem., Int. Ed.*, 2010, **49**, 6260-6266.
14 P. Horcajada, C. Serre, G. Maurin, N. A. Ramsahye, F. Balas, M. a. Vallet-Reg í, M. Sebban, F. Taulelle and G. r. F érey, *J. Am. Chem. Soc.*, 2008, **130**, 6774-6780.
15 L. E. Kreno, K. Leong, O. K. Farha, M. Allendorf, R. P. Van Duyne and J. T. Hupp, *Chem. Rev.*, 2012, **112**, 1105-1125.
16 Z. Xie, L. Ma, K. E. deKrafft, A. Jin and W. Lin, *J. Am. Chem. Soc.*, 2009, **132**, 922-923.
17 Y. Cui, Y. Yue, G. Qian and B. Chen, *Chem. Rev.*, 2012, **112**, 1126-1162.
18 S. M. Cohen, *Chem. Rev.*, 2012, **112**, 970-1000.
19 F. Ke, L. G. Qiu, Y. P. Yuan, F. M. Peng, X. Jiang, A. J. Xie, Y. H. Shen and J. F. Zhu, *J. Hazard. Mater.*, 2011, 196, 36-43.
20 J. G. Nguyen and S. M. Cohen, *J. Am. Chem. Soc.*, 2010, **132**, 4560-4561.
21 A. Huang, W. Dou and J. Caro, *J. Am. Chem. Soc.*, 2010, **132**, 15562-15564.
22 M. J. Ingleson, J. P. Barrio, J. B. Guilbaud, Y. Z. Khimyak and M. J. Rosseinsky, *Chem. Commun.*, 2008, 2680-2682.
23 Y. Lu and W. Chen, *Chem. Soc. Rev.*, 2012, **41**, 3594-3623.
24 M. Zhu, C. M. Aikens, F. J. Hollander, G. C. Schatz and R. Jin, *J. Am. Chem. Soc.*, 2008, **130**, 5883-5885.
25 A. Corma, H. Garc á and F. X. Llabr és i Xamena, *Chem. Rev.*, 2010, **110**, 4606-4655.
26 Y. Huang, Z. Zheng, T. Liu, J. L ü, Z. Lin, H. Li and R. Cao, *Catal. Commun.*, 2011, **14**, 27-31.
27 A. Dhakshinamoorthy and H. Garcia, *Chem. Soc. Rev.*, 2012, **41**, 5262-5284.
28 H. Liu, Y. Liu, Y. Li, Z. Tang and H. Jiang, *J. Phys. Chem. C*, 2010, **114**, 13362-13369.
29 L. Shen, W. Wu, R. Liang, R. Lin and L. Wu, *Nanoscale*, 2013, **5**, 9374–9382.
30 G. Huang, L. Zhang, F. Zhang, and L. Wang, *Nanoscale*, 2014, **6**, 5509–5515.
31 C. Zlotea, R. Campesi, F. Cuevas, E. Leroy, P. Dibandjo, C. Volkringer, T. Loiseau, G. F érey and M. Latroche, *J. Am. Chem. Soc.*, 2010, **132**, 2991-2997.
32 Y. E. Cheon and M. P. Suh, *Angew. Chem., Int. Ed.*, 2009, **48**, 2899-2903.
33 M. Sabo, A. Henschel, H. Frode, E. Klemm and S. Kaskel, *J. Mater. Chem.*, 2007, **17**, 3827-3832.
34 J. Juan-Alcaniz, J. Gascon and F. Kapteijn, *J. Mater. Chem.*, 2012, **22**, 10102-10118.
35 Y. Liu and Z. Tang, *Adv. Mater.*, 2013, **25**, 5819-5825.

36 L. He, Y. Liu, J. Liu, Y. Xiong, J. Zheng, Y. Liu and Z. Tang, *Angew. Chem., Int. Ed*., 2013, **52**, 3741-3745.
37 X. Cheng, A. Zhang, K. Hou, M. Liu, Y. Wang, C. Song, G. Zhang and X. Guo, *Dalton Trans*., 2013, **42**, 13698-13705.
38 T. Ahnfeldt, D. Gunzelmann, T. Loiseau, D. Hirsemann, J. Senker, G. Fe ŕey and N. Stock, *Inorg. Chem.*, 2009, **48**, 3057-3064.
39 T. Loiseau, C. Serre, C. Huguenard, G. Fink, F. Taulelle, M. Henry, T. Bataille and G. Ferey, *Chem. Eur. J.*, 2004, **10**, 1373-1382.
40 R. J. T. Houk, B. W. Jacobs, F. E. Gabaly, N. N. Chang, A. A. Talin, D. D. Graham, S. D. House, I. M. Robertson and M. D. Allendorf, *Nano Lett*., 2009, **9**, 3413-3418.
41 M. Meilikhov, K. Yusenko, D. Esken, S. Turner, G. Van Tendeloo and R. A. Fischer, *Eur. J. Inorg. Chem*., 2010, **2010**, 3701-3714.
42 D. Esken, S. Turner, O. I. Lebedev, G. Van Tendeloo and R. A. Fischer, *Chem. Mater*., 2010, **22**, 6393-6401.
43 H. R. Moon, D. W. Lim and M. P. Suh, *Chem. Soc. Rev.*, 2013, **42**, 1807-1824.
44 C. Battocchio, C. Meneghini, I. Fratoddi, I. Venditti, M. V. Russo, G. Aquilanti, C. Maurizio, F. Bondino, R. Matassa, M. Rossi, S. Mobilio and G. Polzonetti, *J. Phys. Chem. C*, 2012, **116**, 19571–19578.
45 D. Wang, G. Xue, Y. Zhen, F. Fu and D. Li, *J. Mater. Chem*., 2012, **22**, 4751–4758.
46 *NIST X-ray Photoelectron Spectroscopy Database, Version 4.1*; National Institute of Standards and Technology: Gaitherburg, 2012; http://srdata.nist.gov/xps/.
47 R. Matassa, I. Fratoddi, M. Rossi, C. Battocchio, R. Caminiti and M. V. Russo, *J. Phys. Chem. C*, 2012, **116**, 15795–15800.
48 M. Bootharaju and T. Pradeep, *J. Phys. Chem. C*, 2010, **114**, 8328–8336.
49 P. Zhang, C. Shao, Z. Zhang, M. Zhang, J. Mu, Z. Guo, Y. Sun and Y. Liu, *J. Mater. Chem.*, 2011, **21**, 17746–17753.
50 J. Moellmer, E. B. Celer, R. Luebke, A. J. Cairns, R. Staudt, M. Eddaoudi and M. Thommes, *Microporous Mesoporous Mater.*, 2010, **129**, 345-353.
51 S. Besson, T. Gacoin, C. Ricolleau and J.-P. Boilot, *Chem. Commun*., 2003, 360-361.
52 Y. Sun and Y. Xia, *Science*, 2002, **298**, 2176-2179.
53 S. Biswas, T. Ahnfeldt and N. Stock, *Inorg. Chem*., 2011, **50**, 9518-9526.
54 F. Salles, S. Bourrelly, H. Jobic, T. Devic, V. Guillerm, P. Llewellyn, C. Serre, G. r. Ferey and G. Maurin, *J. Phys. Chem. C*, 2011, **115**, 10764-10776.

